Korean J. Chem. Eng., 38(11), 2365-2374 (2021)
DOI: 10.1007/s11814-021-0877-2

pISSN: 0256-1115
eISSN: 1975-7220

Industrial by-product utilized synthesis of mesoporous aluminum silicate sorbent for thorium removal

Sarah Alharthi* and Mahmoud Osman Abd El-Magied,†**

*Department of Chemistry, College of Science, Taif University, P.O. Box 11099, Taif 21944, Saudi Arabia
**Department of Isotope Geology, Research Sector, Nuclear Materials Authority, P.O. Box 530, El Maadi, Cairo, Egypt
(*Received 14 April 2021 • Revised 3 June 2021 • Accepted 22 June 2021*)

Abstract−Recently, there has been an increasing concern in finding sorbents for radionuclide removal from natural sources. AS-BFS sorbent (aluminum silicate composites derived from blast furnace slag) is a suitable candidate for this purpose; due to economic and environmental reasons. Blast furnace slag (BFS) is a by-product of the iron and steel industry plants. The development of a cost-effective route for recycling and utilization assessment of BFS is an urgent task. AS-BFS was prepared from BFS and its physicochemical properties were determined. The elemental composition of the AS-BFS is mainly oxygen (44%), Si (34%), and Al (19%), with traces of titanium, iron, chloride, and calcium. Experimental potentiality regarding sorption characteristics of AS-BFS to thorium ions was explored via the batch method. AS-BFS showed good adsorption capacity for thorium (obtained after 240 min) from aqueous streams (39.7 mg/g). The sorption process is fitted to the mono-layer adsorption model at optimum conditions. It was also proved that adsorption kinetics follows the pseudo-second-order model. The desorption results revealed that thorium ions (93%) could be eluted using 1 M HNO_3. Hence, the research work indicates that the thorium sorption method with AS-BFS is cost-effective, efficient, and recommended for thorium removal from natural sources.

Keywords: Iron By-product, Removal, Mesoporous, Thorium, Isotherms

INTRODUCTION

Thorium is a naturally radioactive element used in various nuclear operations. It has different radioisotopes of mass numbers ranging from 209 to 238; among them, ^{232}Th and ^{230}Th are the most stable isotopes. ^{232}Th is the parent primordial radionuclide, it is 3 to 5 times more abundant than uranium. The major thorium ores are Thorite ($ThSiO_4$, Th wt%=71.59), Thorianite (ThO_2, Th wt%=87.88), Allanite ($Ca(REE,Ca)Al_2(Fe^{2+},Fe^{3+})(SiO_4)(Si_2O_7)O(OH)$, Th wt%= 0.1-2), Monazite ($(Ce, La, Nd, Th)PO_4$, Th wt%=7.83), and Zircon ($ZrSiO_4$) [1-5]. The radioactivity inherent in thorium is a major factor impeding its use in industrial applications, but these properties may also make it a candidate for use as an alternative nuclear fuel in nuclear reactors in place of uranium. It is predicted that thorium may be able to replace uranium in the future as nuclear fuel in nuclear reactors. Thorium's long-term use would improve dramatically if it became usable as a nuclear fuel. Thorium compounds have several uses such as catalysts, high-temperature ceramics, welding electrodes, electron tubes, photoconductive films, airport runway lighting, high-refractive glass, detectors, and X-ray tubes. Thorium use is normally restricted in most of these materials due to issues about its natural radioactivity.

Contamination of water bodies with radionuclides has become a significant and emerging issue increasingly important during the past few years [1,5,6]. In addition to thorium natural sources, thorium applications produce different thorium liquid and solid waste which may contaminate the aquatic system. Thorium is non-essential metal and may cause several health impacts. The U.S. Environmental Protection Agency (EPA) has set a maximum contaminant level for thorium in drinking water at 15 pCi/L (picocuries per liter) [7-9]. Thorium is removed from the aqueous solution by different separation methods. The key methods for thorium recovery are solvent extraction [10], ionic liquid [11], sorption and ion exchange [4,6,12,13], and precipitation [5].

Sorption is the primary separation method for thorium because of its realistic, environmental and strategic advantage [4,6]. Sorption mechanisms usually involve all ways in which substance ions or molecules (adsorbate or sorbate) tie the surface or volume of other material (adsorbent or sorbent). As a result, sorption affects the composition of an adsorbate on the surface of an adsorbent. Sorption then transfers the compound concentration (or adsorbate) from the liquid phase (or adsorption medium) to another solid phase (or adsorbent) [14,15].

The production of solid absorbers capable of remediation of thorium is one of the safest methods of mitigating water pollution. The finding of replacements for thorium rehabilitation from natural sources has recently become more knowledgeable. Recent interest has been placed on the development of sorting systems that use natural thorium separation systems of metal oxide, chitosan, alumina, silica, activated carbon [16,17]. Among natural adsorbents, silica and alumina-based sorbents have received considerable attention because of their mechanical, chemical, and textural properties in addition to availability, nontoxicity, and cheap price [14,18-23]. Mesoporous materials have attracted expanding importance within

†To whom correspondence should be addressed.
E-mail: mahmoud_nma@yahoo.com

the past years and have seen various potential uses in different fields. Mesoporous silica and/or alumina-based adsorbents are some of the most promising materials used in environmental remediation and nuclear engineering for thorium and uranium separation [20, 21,23].

High quantities of by-products or slags (mainly solid products) are produced by iron and steel-making plants, along with pig iron and steel as the main products. Research on waste recycling systems, driven by environmental and economic considerations, has recently gained considerable interest. Blast furnace slag (BFS) is a by-product of iron and steel industry plants. The development of a cost-effective route for recycling and utilization assessment of BFS is an urgent task. BFS contains variable amounts of elements (such as iron, silica, alumina, manganese, calcium, magnesium) in the form of oxides, ferrite, aluminate, and silicate, in addition to some heavy metal elements (such as Cr, As, Cd, Pb). Generally, BFS is used in concrete, agriculture as a soil conditioner and as a fertilizer, and construction industries. The heavy metal ions in the BFS may have adverse effects on human health and aquatic life via a potential seawater/groundwater contamination, and urgent problems such as storage and regulations. Hence, the development of new and advanced recycling approaches for waste slags has been required to promote the sustainable development of the iron and steel industry. Also, in agriculture uses, these slags can induce contamination of soil by some heavy metal elements found in slags. BFS recycling has an important role in reducing waste from the environment.

This research was dedicated to the recycling of BFS. The present work is intended to prepare solid sorbent derived from blast furnace slag for thorium inclusion from its solution. The chemical component of BFS from iron and steel making slags is less variable and mainly consists of CaO (40%), SiO_2 (35%), Al_2O_3 (15%), MgO (5%), FeO (1.5%), Ti (0.8%), and Mn (0.3%). BFS was thus utilized as a solid sorbent source. Thorium is stripped out of natural water by the sorbent, AS-BFS. The physicochemical properties of the obtained sorbent were determined using instrumental analysis. The impacts of different vital thorium sorption parameters were optimized. It is yet another object of the instant research to provide a complete kinetic and isotherm characterization of the used process. This is achieved by the treatment of the batch results by various models. Another object is to study the reusability of the waste-based adsorbent.

MATERIALS AND METHODS

1. Synthesis of AS-BFS

From the Helwan factory for iron and steel industries, Cairo, Egypt, the used BFS was produced. The raw blast furnace slag (BFS) was first washed, with distilled water, and dried (120 °C) for 24 hours. The dried blast furnace slag was ball-milled at 500 rpm (for 30 min) and sieved using an 80-μm sieve then dissolved 20 g of fine BFS powder in 400 mL of 3 M HCl (37%, Aldrich product) with continuous stirring for 3 h. A 2 M NaOH (97%, Aldrich product)

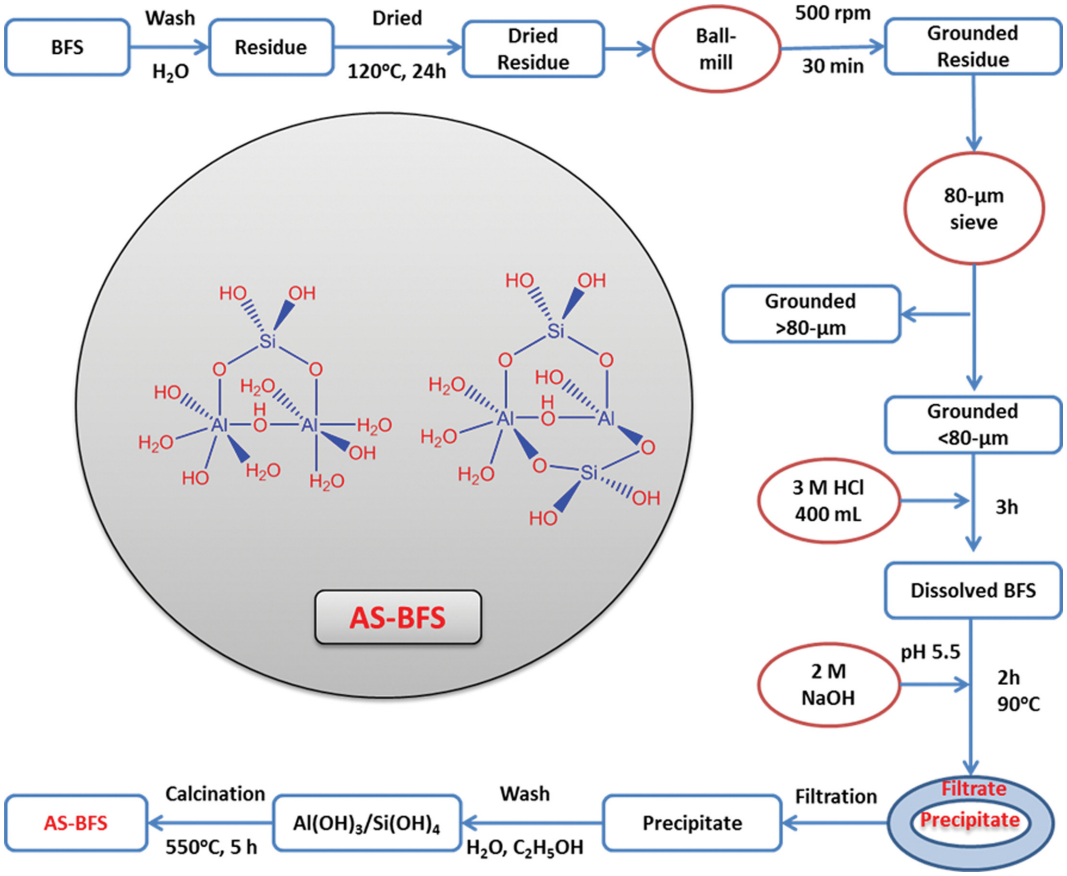

Fig. 1. AS-BFS synthesis.

solution was added dropwise to the previous solution to get a white precipitate (pH 5.5±0.1). The obtained precipitate of aluminum hydroxide and silicon hydroxide was stirred for 2 h at 90 °C and aged at 50 °C overnight. The slurry was filtered, washed a few times with de-ionized water until filtrate free-chloride, then twice with ethanol. The precipitate was filtered, washed, and dried (110 °C; 4 h). The obtained solid was calcined at 500 °C (5 h) to obtain pale grey powder (AS-BFS). The AS-BFS was applied for the adsorption of thorium ions from their aqueous solution. Fig. 1 illustrates a cost-effective route for recycling and utilization assessment of BFS to produce an aluminum silicate adsorbent (AS-BFS).

2. Adsorption Measurements

A stock solution of Th(VI) (1,000 mg/L) was prepared by dissolving 2.46 g of thorium nitrate in 1,000 ml of distilled water. Experiments on batch adsorption were done by shaking vials containing the desired AS-BFS dose in a predetermined concentration of thorium solution, at pH range 1-5, for different time intervals. For a series of bottles containing AS-BFS (10 mg) suspension, 20 ml of thorium-containing solution (50 mg/L) was applied to each bottle at various pH values (1-5). For specific experiments, the pH was initially adjusted to a fixed value with solutions of NaOH or HNO_3. The bottles were shaken at 25 °C, 300 rpm, for 24 h then they were filtered and the residual thorium concentration was determined in the filtrate. Thorium ions were determined using UV/Vis spectrophotometer of type Unicam UV2-100, UK. The concentration of thorium was quantified spectrophotometricaly at λ_{max} 540 nm using the Thoron I method (Supplementary Information, Fig. S1) [24].

For kinetic studies, 20 mL of the thorium solution (100 mg/g) interacted with 0.01 g of the sorbent at pH (4) for (10-240) min. We filtered the AS-BFS and the thorium concentrations into the filtrate were analyzed and used in kinetic analysis. The thorium ion concentrations of the medium were taken against the time for kinetic models.

Impact of variable thorium concentrations on the sorption by the AS-BFS was studied, suspensions containing AS-BFS 0.01 g in a series of vials, in each bottle, a solution of 20 mL of 10-300 mg/L of thorium at pH 4 for was stirred for 4 h. The residual thorium ion concentration in the samples obtained after equilibrium was analyzed using a spectrophotometer at λ_{max} 540 nm. In the experiments, the amount of thorium accumulated on the sorbent (uptake, q_e) was calculated by using Eq. (1) from the variation between initial thorium concentration (C_i, mg/L) and that remaining in solution (V, L) after equilibrium with the sorbent (C_e, mg/L) [6].

$$\text{Uptake, } q_e = \frac{\left(C_i\left(\frac{mg}{L}\right) - C_e\left(\frac{mg}{L}\right)\right) \times V(L)}{\text{mass of adsorbent (g)}} \quad (1)$$

To measure various kinetics and isothermal parameters, the data obtained was checked by several models.

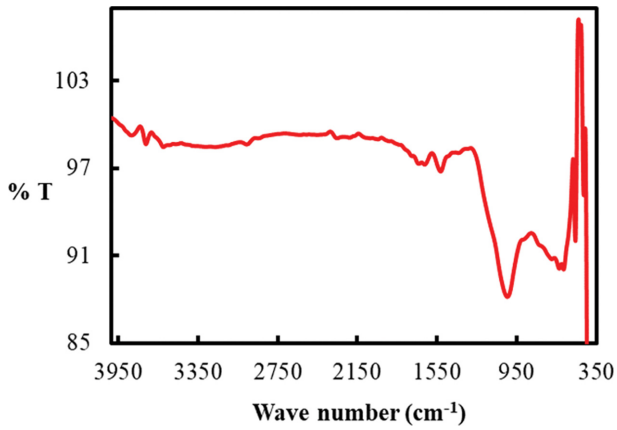

Fig. 2. The FTIR spectrum of AS-BFS.

RESULTS AND DISCUSSION

1. AS-BFS Characterization

The AS-BFS adsorbent was prepared simply and easily from BFS waste of the iron and steel industry (Fig. 1). Dynamic light scattering analysis (DLS) was performed to characterize the size of AS-BFS. The average size of the AS-BFS particles was 1,877 nm. The FTIR spectrum of AS-BFS (Fig. 2) showed the OH bands at 3,215 and 3,760 cm^{-1} (stretch and bend), H_2O band at 1,692 cm^{-1} (stretch), and CO_2 (adsorbed from the air) band at 1,545 cm^{-1}. The spec-

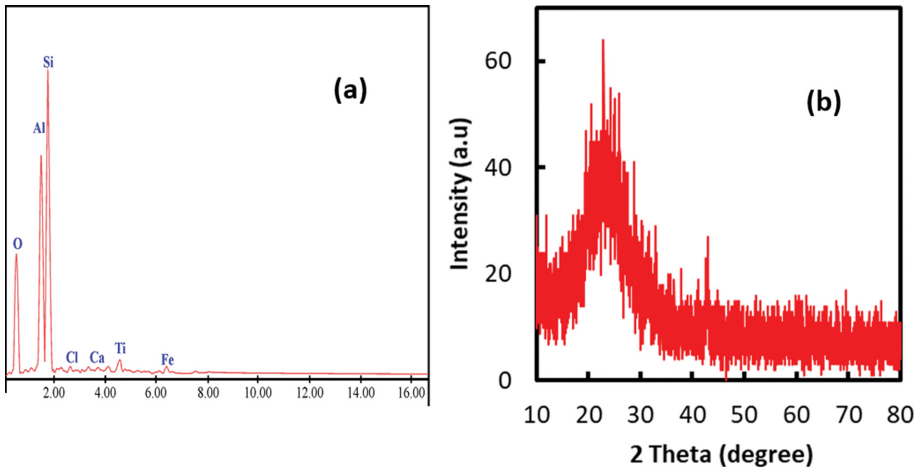

Fig. 3. EDX analysis (a) and XRD (b) patterns of the AS-BFS.

trum also showed the (Si/Al=O) and (Si-O-Si) bands at 1,054 cm^{-1} (stretch), Al-O-Si absorption bands 678 cm^{-1} (stretch), Al-O_6 band at 636 cm^{-1} (stretch and bond), and the Al-O and Si-O absorption bands at nearly 407, 447, and 512 cm^{-1} (stretch) [25].

Fig. 3 shows the EDX analysis and XRD patterns and of the AS-BFS. The EDX analysis (Fig. 3 (a)) shows that the elemental composition of the AS-BFS is mainly oxygen (44%), Si (34%) and Al (19%), with traces of titanium (1.4%), iron (0.6%), chloride (0.4%), and calcium (0.2%). Fig. 3(b) shows that the AS-BFS is amorphous aluminum silicate or calcium aluminum silicate (broad peak between 22 and 35°) [26]. Other researchers [27,28] also observed similar results for aluminum silicate composites prepared from other sources. The wide-angle XRD patterns indicated that the AS-BFS sample consisted of amorphous aluminum silicate composites [29].

The N_2 adsorption-desorption model of AS-BFS was measured at 25 °C (Fig. 4(a)). The model gives type IV isotherm (at P/P_o> 0.48 up to P/P_o=0.97) which indicates homogeneous pore shapes [30]. This type of isotherm is commonly observed in mesoporous materials. The existence of mesopore in AS-BFS was also verified by the distribution of the pore as the majority of the AS-BFS pores fall within the 3.3-4.1 nm range, Fig. 4 (inset) [31,32]. The specific surface area of AS-BFS is 36.5 m^2/g, which is a good value compared to that for adsorbents prepared by others such as alumina-silica gel (16.7 m^2/g) [33], synthetic aluminum silicate (16.7 m^2/g) [34]. aluminophosphate (90 m^2/g) [35].

Fig. 4(b) shows the thermogravimetric behavior (TGA) of AS-BFS. One main observed weight-loss stage (11%) of prepared AS-BFS composite happened below 100 °C, which should have been due to the evaporation of physically adsorbed water molecules. The second loss stage peak (1%) appeared at 270 °CC introduces the dehydration of the aluminum hydroxide $Al(OH)_3$ to Al_2O_3 [36].

2. Optimization of Thorium Sorption by AS-BFS

2-1. Impact of pH on Thorium Uptake by AS-BFS

To understand the solution's pH role in the thorium uptake capacity, different pH values were tested (1-5), Fig. 5(a). The adsorption sites of AS-BFS with low pH levels compete with H^+ ions (from the solution), thus thorium adsorption decreases. Increasing the adsorption medium pH increases the thorium absorption. The increase in thorium uptake might be due to the reduction in AS-BFS surface protonation at higher pH values. The experimental results indicate an optimal pH value of 3.5-4. At the optimum pH, the uptake capacity of thorium is 29.6 mg/g (Fig. 5(a)).

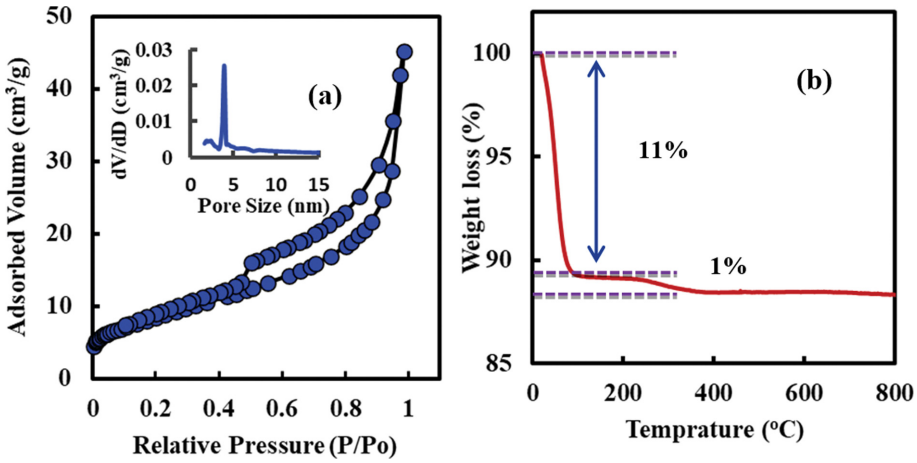

Fig. 4. (a) BET (and pore diameter (inset)) and TGA analysis of the AS-BFS sorbent.

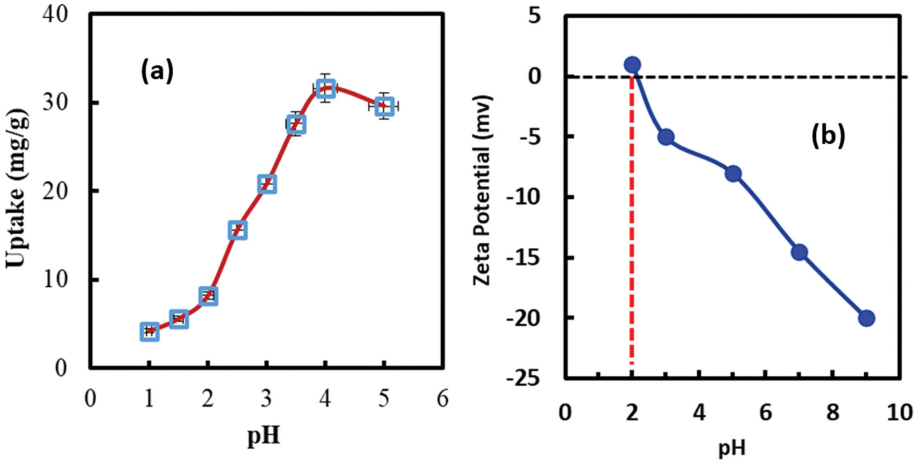

Fig. 5. Impact of pH on thorium uptake by AS-BFS (a) and zeta potential measurements of the AS-BFS (b).

Fig. 5(b) shows the Zeta potential measurements of the AS-BFS at various pH. The zero point of charge of the AS-BFS is at about pH 2, so the surface AS-BFS is positively charged at pH<2 and negatively charged at pH>2. This value gives AS-BFS the capability to adsorb cations at pH>2. The lower uptake at pH≤2 may be due to repulsion between thorium ions and the positively charged AS-BFS surface, in addition to competition with H^+ ions (from the adsorption solution) for the AS-BFS active sites. As the pH value rises, the AS-BFS surface becomes positively charged and competition with H^+ ions decreases; consequently, the uptake of thorium ions by AS-BFS increases.

Thorium adsorption relies on pH values and can be correlated with solution chemistry. At lower pH values (≤4), thorium presents as Th^{+4}, $Th(OH)^{+3}$, $Th(OH)_2^{+2}$ and $Th(OH)_3^{+}$ species. These cationic species can interact with the adsorbent, so uptake increases. At higher pH values (>4) different polynuclear thorium species are formed (i.e., $Th_4(OH)_{12}^{4+}$ $Th_6(OH)_{15}^{9+}$). These species have a lower tendency to interact with the adsorbent, so uptake decreases. A further increase in pH led to the precipitation of thorium hydroxide [37].

On the other hand, according to Beardmore et al. [38], two suggested hydroxyl aluminosilicate structures may be formed (Fig. 1). The $Al(OH)_3$ dimer with either single or double hydroxy bridge, and incorporating $(Si(OH)_4)$ into the structure in the form of Al-O-Si-O-Al. The other coordinating sites in silica were linked to O-H groups, $Si(OH)_4$ [39]. The AS-BFS surface charges became more negative with increasing solution pH (point of zero charges of AS-BFS is 2.0), which enhanced the interaction between the thorium cationic species and the negatively charged AS-BFS surface charges.

The suggested thorium adsorption process on AS-BFS can be caused by either coordination (Eq. (2)) or by the exchange of bound H^+ ion on the AS-BFS surface with thorium (as suggested by Eq. (3)).

$$Th^{4+}+[-AS-BFS-OH]\rightarrow[-AS-BFS-O-Th^{4+}\ H^+] \quad (2)$$

$$Th^{4+}+x[-AS-BFS-OH]\rightarrow Th[-AS-BFS-O]_x^{4-\times}+xH^+ \quad (3)$$

2-2. Effect of Initial Thorium Ion Concentration

The effect of initial thorium ion concentration (C_i) provides the main driver to resolve all thorium ion mass transfer resistance between the liquid/solid phases. At various thorium concentrations, different q_e values are achieved; the larger the thorium C_i, the greater the number of thorium ions bound to the AS-BFS surface at equilibrium (Fig. 6).

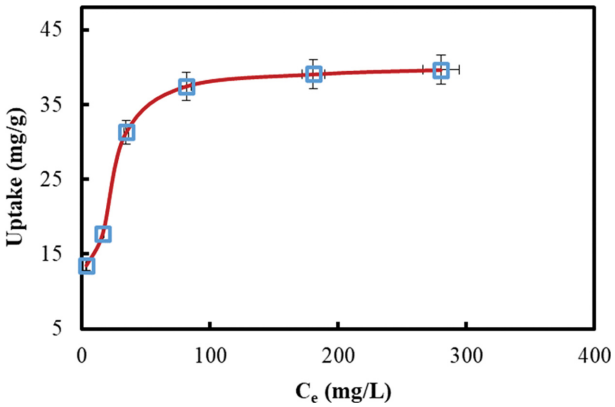

Fig. 6. Impact of Th(VI) concentration on thorium uptake by AS-BFS.

Table 1. Comparison of various adsorbents capacities for U(VI) ions

Adsorbent	Sorption capacity (mg/g)	Reference
Zeolite	9.2	40
gibbsite	0.9	41
tin oxide	62.5	42
Alumina	15.3	43
AS-BFS	39.7	This work

It is observable that adsorption capacity increases with the rise in the initial thorium concentration (Fig. 6). Higher C_i of thorium enhances adsorption potential (39.68 mg/g); this may be because the reaction with the same active site is possible for increased thorium ions. As compared to other natural adsorbents (Table 1), AS-BFS has a large capacity for thorium ions; on the other hand, its chemical stability, low cost, and ease of synthesis suggest that it may be a viable adsorbent in thorium removal technology.

2-3. Adsorption Isotherms

Isotherm is an empirical relation that predicts how much solid sorbent can adsorb solute. The adsorption isotherm as a graph describes the link of the adsorbed quantity by a unit weight adsorbent and the adsorbed quantity remaining in a test medium. The adsorption isotherm is based on knowledge unique to each system, and the isotherm must be calculated for all applications. Therefore, the adsorption isotherm maps the distribution of adsorbate at different equilibrium concentrations between the liquid/solid phases. An adsorption isotherm, in addition to offering a designation of the method, studied succinctly, shows how effective this is for commercial application for the specific solute.

Two models have assessed the monolayer formation of thorium over AS-BFS surface, Langmuir and Dubinin-Radushkevich isotherms [4,6,44,45]. Langmuir's theory (Eq. (4)) is limited to situations where just a monolayer of ions or molecules adsorbs on an adsorbent surface. In monolayer adsorption, at moderate concentrations, the adsorbed quantity reaches a maximum value, corresponding to the full surface coverage of the adsorbent.

$$\text{Langmuir model: } \frac{C_e}{q_e}=\frac{C_e}{Q_L}+\frac{1}{K_L Q_L} \quad (4)$$

From the Langmuir plot's intercept and the slope, Q_L and K_L were derived (Fig. 7(a), Table 2). The agreement between the Q_L and q_e values, plus R^2>0.997, indicates the ability of this model to explain the adsorption process with a high surface coverage (Langmuir surface coverage, $\theta=K_LC_i/(1+K_LC_i)$) of AS-BFS ranged between (0.45-0.96), (Fig. 7(b)). The AS-BFS's degree of suitability to thorium ions was predicted by the Langmuir separation factor (R_L) values. The adsorption of thorium ion by AS-BFS is desirable when the R_L values are within the range $0<R_L<1$. As seen in Fig. 7(c), R_L values fall in the range of 0.04-0.6, which suggests a suitable adsorption process.

Another isotherm that describes the monolayer adsorption system is the Dubinin-Radushkevich isotherm (D-R). This isotherm is a temperature-dependent model for the estimation of apparent

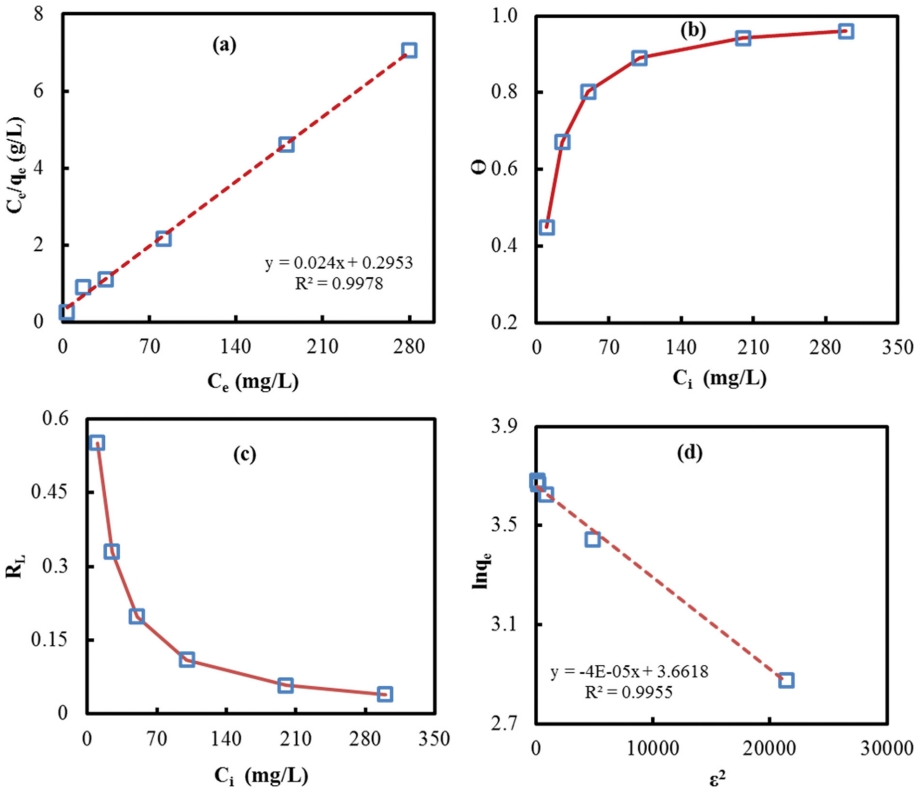

Fig. 7. Langmuir adsorption isotherm (a), Langmuir surface coverage (b) Langmuir separation factor (c), and Dubinin-Radushkevich adsorption isotherm (d) for thorium ion adsorption by AS-BFS.

Table 2. Adsorption isotherms of thorium ion adsorption on AS-BFS

Isotherm model	Parameters	Value
Langmuir	Q_L	41.67
	K_L	0.081
	R^2	0.9978
D-R	q_{DR}	38.93
	K_{DR}	4.0 E-08
	E	3.54
	R^2	0.9955
Freundlich	K_F	10
	1/n	0.267
	R^2	0.9012
Temkin	β	6.64
	A_T	2.005
	R^2	0.9107

adsorption energy (E); also, this isothermal model is used to estimate the characteristic porosity. The adsorption is commonly used with Dubinin-Radushkevich isotherm by Eq. (5) and (6).

$$\text{Dubinin-Radushkevich model: } \ln q_e = \ln q_{DR} - K_{DR}\varepsilon^2 \quad (5)$$

$$\text{The apparent adsorption energy: } E = \frac{1}{(2K_{DR})^{1/2}} \quad (6)$$

Constants such as q_{DR} (D-R capacity, mg/g) and K_{DR} (D-R constant, mol^2/kJ^2), and E (KJ/mol) were determined from the D-R plot (Fig. 7(d)), using Eqs. (4) and (5) above, q_{DR} was determined to 38.93 mg/g, and K_{DR} (4×10^{-8}) and, E=3.54 KJ/mol indicating a physic-sorption process.

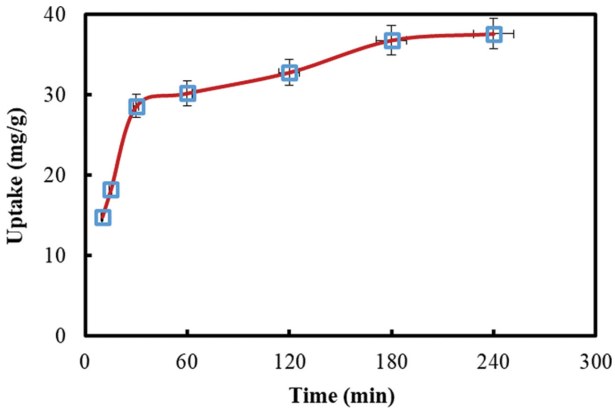

Fig. 8. Effect of time on thorium ion adsorption by AS-BFS.

Two models were used to test the multilayer formation of thorium over AS-BFS surface, Freundlich (Eq. (S1)) and Temkin (Eq. (S2)) isotherms (Supplementary information file), and the corresponding parameters were inserted in Table 2. The results obtained indicate the incompatibility of these models to explain the thorium ion adsorption by AS-BFS.

2-4. Impact of Time on the Mechanism of Adsorption

To determine the kinetic parameters necessary to design an ad-

sorption plant, an investigation of the adsorption kinetics is required. The batch system is widely used for kinetic investigations. In this system, 0.01 g of adsorbent and 20 mL solution of 100 mg/g initial thorium concentration were mixed and stirred, while the time variation of concentration was taken as output (Fig. 8).

Initial fast thorium uptake can be caused by the presence of vacancy sites on the AS-BFS surface. As the thorium ions filled up more adsorption sites, the uptake rate became less efficient; this slow uptake may be due to repulsive forces between the adsorbed thorium ions and to the diffusion of thorium ions into the AS-BFS inner surfaces.

2-5. Kinetic Studies

When an adsorption process starts, the reverse is also initiated, desorption or freedom of adsorbed molecules (i.e., coordinated water molecules) from the AS-BFS surface starts. After a few times, equilibrium is attained, the numbers of adsorbed thorium on the AS-BFS surface at a time unit corresponds to the number of molecules desorbed or taken off the AS-BFS surface, and the thorium adsorbed no longer varies in time. It was found that in the first 30 minutes, the uptake was quick. The AS-BFS surface was packed with more time and the plateau was obtained after 240 min.

The film, external, porosity diffusion, and/or adsorption regulate the kinetics of thorium adsorbed from the solution (solvent-solute process). Four kinetic models were used to interpret the findings. To calculate thorium distribution, linear regression of different kinetic models was chosen, adsorption methods were tested

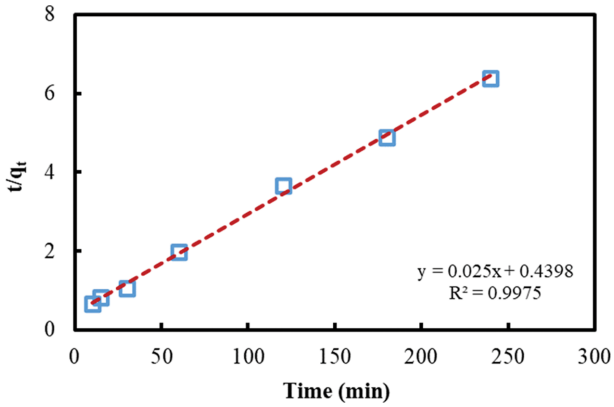

Fig. 9. Pseudo-second-order model for thorium ion adsorption by AS-BFS.

mathematically; the exactness and theory of these kinetic models were validated. The earliest model of the rate of liquid/solid adsorption was introduced in the Lagergren model (Supplementary information file, Eq. (S3)). The rate kinetic evaluation was also done by the pseudo-second model using Eq. (7) [44,45].

$$\frac{t}{q_t} = \frac{1}{k_2 q_2^2} + \frac{1}{q_e} t \quad (7)$$

q_2 (pseudo-second model adsorption capacity) and k_2 (rate con-

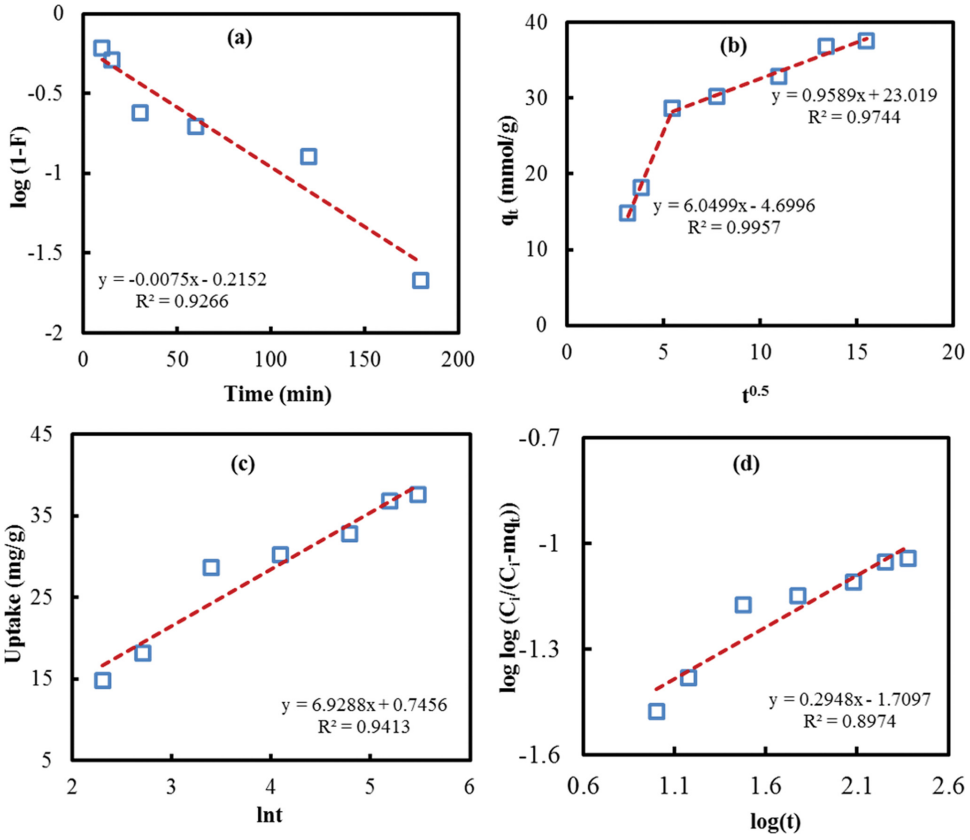

Fig. 10. Liquid film diffusion model (a), Intraparticle film diffusion model (b), Elovich model (c), and Bangham model (d) for thorium ion adsorption by AS-BFS.

stant) were acquired from the pseudo-second-order model plot (Fig. 9, (t/q_t) vs. (t)). The plot gives a straight line with a higher R^2 value, relative to pseudo-first-order, the thorium adsorption complied with the pseudo-second model. The findings demonstrate that the pseudo-second-order can be used for thorium/AS-BFS adsorption characterization with a strong regression coefficient value (>0.99).

If the adsorbent is nonporous, adsorption occurs only on the external surface, the adsorption rate will be controlled by film diffusion onto the aqueous film surrounding the adsorbent. If the adsorbent is porous, adsorption may occur onto the surface and pores. Two processes, either film diffusion or intraparticle diffusion, typically regulate the adsorbent rate within porous adsorbents. Both mechanisms are in practice present, but one mechanism is generally prevalent. Film diffusion primarily depends on particle size, solution composition, film thickness, and the effective coefficient of film diffusion of the ions.

The boundary layer can play a major role in the adsorption process during the transport of thorium-ion species from the bulk liquid phase into the AS-BFS surface. The time adsorption data can be checked by applying the liquid film diffusion equation (Eq. (8)).

$$\log(1-F) = -\frac{K_{LF}}{2.303}t \quad (8)$$

The value of K_{LF} is obtained from the log(1−F) versus (t), where F is fractional attainment at equilibrium ($F=q_t/q_e$), Fig. 10(a). In general, the adsorption processes which are regulated by diffusion by the liquid film at the adsorbent interface describe when the plots contain a null intercept line. The liquid film diffusion rate constant (K_{LF}) is 0.017; the plot gives a straight line ($R^2>0.92$) that refers to a boundary layer effect; the small intercept (−0.215) indicates that the film diffusion in the studied adsorption process is not the only slow step. Intraparticle diffusion refers to the rate of diffusion of ions or molecules in the adsorbent matrix. Intraparticle diffusion is typically the rate-control step (slow) for porous adsorbents and is measured by the Weber-Morris equation, Eq. (9). Intraparticle diffusion relies on the fixed charge concentration and the particle-diffusion coefficient, which differ according to the composition of the adsorbent. Weber-Morris equation or intraparticle diffusion concerns the diffusion rate of adsorbate within the adsorbent matrix, Eq. (9) [44].

$$q_t = k_{id}t^{1/2} + C \quad (9)$$

Using Eq. (9), initial uptake constant k_{id} (mg thorium ion per gram AS-BFS) can be determined from the q_t versus the $(\text{time})^{1/2}$ slope. The intraparticle diffusion (IPD) is the slow phase on a single linear plot, where multi plots suggest mixed effects to be rate-limiting steps (Fig. 10(b)). The Weber-Morris model gives two lines with intercepts of –4.6996 and 23.019; R^2 values of 0.9957 and 0.9744, Table 3. The value of the rate constant of the first linear portion (K_{id}) is 0.3.46 mg/g.min$^{0.5}$. The presence of two straight lines indicates that intraparticle film diffusion does not have much role in controlling the reaction. The results refer to the effect of both boundary layer (first curve portion) and intraparticle or pore diffusion (second curve portion) in the adsorption process; therefore, the adsorption process is controlled by mixed effects.

Elovich equation is valuable when the thorium interaction with the adsorbent active sites is the slow step [44-46]; Elovich equation is given by Eq. (10).

$$\text{The Elovich model: } q_t = \frac{1}{\beta}\ln(\alpha\beta) + \frac{1}{\beta}\ln(t) \quad (10)$$

Using Eq. (10), and q_t versus ln(t), Fig. 10(c) initial adsorption rate (α, mg/g·min) and Elovich constant (β, g/mg) can be calculated. The large difference between the calculated values of α and experimental q_e suggests that the adsorption mechanism is not defined by the Elovich model very well. Bangham's model applies to adsorption schemes in which the slow phase is the IPD. The adsorption data for the Bangham model were added according to Eq. (11) [44, 46].

$$\log\left(\log\left(\frac{C_i}{C_i - mq_t}\right)\right) = \log\left(\frac{mK_B}{2.303\ V}\right) + \alpha\log t \quad (11)$$

where (m) is the AS-BFS weight per liter of thorium solution (g/L), the constants of Bangham are α and K_B. Fig. 10(d) shows the plots of the adsorption time data according to the Bangham model. The Bangham model suggests that boundary layer diffusion participates in the adsorption, but not the only one rate-determining step; a linear plot with zero intercepts refers to an adsorption process controlled by that intraparticle diffusion only, otherwise film diffusion plays a factor in the process. The straight line with a low R^2 value (0.8974) indicates that pore diffusion may not be the slow step in the reaction rate. Also, the plot has intercept −1.7, and therefore, the adsorption process is controlled by mixed effects.

Based on the previously discussed results, which are detailed in Table 3, it is clear that the values of R^2 are in the order 0.9975 (pseudo-second-order), 0.9957 (Weber-Morris model), 0.9413 (Elovich model), 0.9266 (pseudo-first-order), 0.9266 (Liquid film diffusion model), and 0.8974 (Bangham kinetic model). Thus, the compatibility of these models with the outcome of the kinetic data will follow the

Table 3. Kinetic models parameters for the Th(IV) adsorption on AS-BFS

Model	Parameters	Value
Pseudo-first-order	q_1 (mg/g)	22.9
	k_1 (min^{-1})	0.017
	R^2	0.9266
Pseudo-second-order	q_2 (mg/g)	40
	K_2 (g/mg·min)	0.001
	R^2	0.9975
Liquid film diffusion model	K_{LF}	0.017
	R^2	0.9266
Weber-Morris model	K_{id}, (mg/g·$\text{min}^{0.5}$)	6.05, 0.96
	C	−4.7, 23.02
	R^2	0.9957, 0.9744
Elovich model	β (g/mg)	0.14
	α (mg/g·min)	7.72
	R^2	0.9413
Bangham kinetic model	K_B	8.99
	α	0.29
	R^2	0.8974

same order as follows: Pseudo-second-order>Weber-Morris model> Elovich model>Pseudo-first-order>Liquid film diffusion model> Bangham model.

3. Thorium Desorption and AS-BFS Regeneration

Desorption and recycling of adsorbents used ensures cost-effectiveness, limited cost of disposal, and eliminates environmental risks of thorium ions loaded on AS-BFS. The elution of thorium ions from the loaded AS-BFS was studied using a batch system. AS-BFS (5 g) was treated with 1 M HNO_3 solution (100 mL) to recover thorium ions. After 2 h, the solution was filtered and the eluted thorium ions were determined. A total of 93% of the loaded thorium ions were eluted. After washing the AS-BFS with H_2O to pH 7, it is regenerated again and is thus ready for further use in thorium sorption. In the second and third runs, the uptake capacity is 32.2 and 23.4 mg/g, respectively.

4. Application

Groundwater is used for drinking and other human activities in southwestern Sinai, Egypt. A water sample from southwestern Sinai (Wadi Naseib area) was treated with AS-BFS at its natural pH value. The sample was analyzed before and after treatment by inductively coupling plasma optical emissions. The non-treated sample shows thorium, nickel, copper, cadmium, lead, and iron of 0.3, 17.6, 0.02, 0.01, 0.09, and 2.07 mg/L. After treatment, these values were decreased to 0.05, 8.4, 0.01, 0.007, 0.03, and 0.5 mg/L, respectively. These results suggest the promising application of the AS-BFS in the water treatment field.

CONCLUSIONS

Mesoporous aluminum silicate sorbent (AS-BFS) was developed from an iron industrial by-product and applied for thorium sorption from its aqueous solutions. The chemical component of BFS consists mainly of Ca, Si, Al, Mg, Fe, Ti, and Mn oxides. The EDX analysis of the AS-BFS shows that the elemental composition is mainly oxygen, silicon, and aluminum, with traces of titanium, iron, chloride, and calcium. The XRD patterns show that the AS-BFS consists of amorphous aluminum silicate composites. The N_2 adsorption-desorption isotherm of AS-BFS gives type IV isotherm (at P/P_o>0.48 up to P/P_o=0.97) indicates homogeneous pore shapes. The existence of mesopore in AS-BFS is also verified by the distribution of the pore (3.3-4.1 nm). The relevant conditions for the thorium sorption of (pH, time, concentration, and reusability) were studied and optimized. Furthermore, kinetic and isotherm modeling were tested to determine the nature of the thorium/AS-BFS interaction. The adsorption of thorium on AS-BFS was found strongly affected by initial pH and thorium concentration. The maximum uptake capacity is obtained after 240 min. AS-BFS showed high uptake capacity of 39.67 mg of Th(IV) ions per gram of AS-BFS. The overall kinetic analyses refer to pseudo-second-order adsorption of thorium on AS-BFS controlled by mixed steps. The suggested mechanism of thorium adsorption on AS-BFS may be due to either coordination or by the ion exchange on the AS-BFS surface with thorium. The results show that D-R and Langmuir isotherms are applicable to characterize the monolayer surface coverage of AS-BFS by thorium ions. Temkin and D-R parameters indicate the physical adsorption of thorium on the AS-BFS surface. The desorption results revealed that thorium ions could be eluted using 1 M HNO_3. Hence, the research work conveys that the proposed adsorption method using AS-BFS is suitable for the thorium sorption from contaminated water bodies.

CONFLICT OF INTEREST

The authors declare that they have no known competing financial interests or personal relationships that could have appeared to influence the work reported in this paper.

ACKNOWLEDGEMENTS

The authors would like to thank Taif University Researchers Supporting Project number (TURSP-2020/200), Taif University, Taif, Saudi Arabia for supporting this project.

SUPPORTING INFORMATION

Additional information as noted in the text. This information is available via the Internet at http://www.springer.com/chemistry/journal/11814.

REFERENCES

1. D. Lancmuir and J. S. Herman, *Geochim. Cosmochim. Acta*, **44**, 1753 (1980).
2. H. G. A. Dill, *Arab. J. Geosci.*, **4**, 123 (2011).
3. A. Vertes, S. Nagy, Z. Klencsar, R. G. Lovas and F. Rosch, *Handbook of nuclear chemistry*, Springer US, New York, (2010).
4. M. O. Abd El-Magied, A. A. Tolba, H. S. El-Gendy, S. A. Zaki and A. A. Ati, *Hydrometallurgy*, **169**, 89 (2017).
5. F. Habashi, *Handbook of extractive metallurgy*, WILEY-VCH, Weinheim, Germany (1997).
6. S. A. Sadeek, E. M. Moussa, M. A. El-Sayed, M. M. Amine and M. O. Abd El-Magied, *J. Dispersion Sci. Technol.*, **35**, 926 (2014).
7. Agency for Toxic Substances and Disease Registry (ATSDR), Toxicological Profile for thorium, Atlanta, GA: U.S. Department of Health and Human Services, Public Health Service (1990).
8. EPA, Drinking water standards and health advisories, Washington, DC: U.S. Environmental Protection Agency, Office of Water, EPA822S12001 (2012).
9. FDA, Subpart B - Requirements for specific standardized beverages, Bottled water, U.S. Food and Drug Administration, Code of Federal Regulations 21 CFR 165.110 (2017).
10. N. T. Hung, L. B. Thuan, T. C. Thanh, M. Watanabe, D. V. Khoai, N. T. Thuy, H. Nhuan, P. Q. Minh, T. H. Mai, N. V. Tung, D. T. T. Tra, M. K. Jha, J. Y. Lee and R. K. Jyothi, *Hydrometallurgy*, **198**, 105506 (2020).
11. Z. F. Akl and M. A. Hegazy, *J. Environ. Chem. Eng.*, **8**, 104185 (2020).
12. D. Yuan, S. Zhang, J. Tan, Y. Dai, Y. Wang, Y. He, Y. Liu and X. Zhao, *Sep. Sci. Technol.*, **237**, 116379 (2020).
13. D. Yuan, S. Zhang, Z. Xiang, Y. He, Y. Wang, Y. Liu, X. Zhao, X. Zhou and Q. Zhang, *ACS Appl. Mater. Interfaces*, **11**, 24512 (2019).
14. J. D. Seader and E. J. Henley, *Separation process principles*, John Wiley & Sons, Inc., New York (2006).

15. E. Worch, *Adsorption technology in water treatment-fundamentals, processes, and modeling*, Germany. Walter de Gruyter, GmbH & Co. KG, Berlin (2012).
16. B. R. Broujeni, A. Nilchi and F. Azadi, *Environ. Nanotechnol. Monit. Manage.*, **15**, 100400 (2021).
17. M. Metaxas, V. Kasselouri-Rigopoulou, P. Galiatsatou, C. Konstantopoulou and D. Oikonomou, *J. Hazard. Mater.*, **97**, 71 (2003).
18. L. Dolatyari, M. Shateri, M. R. Yaftian and S. Rostamnia, *Sep. Sci. Technol.*, **54**, 2863 (2019).
19. Z. Dousti, L. Dolatyari, M. R. Yaftian and S. Rostamnia, *Sep. Sci. Technol.*, **54**, 2606 (2019).
20. L. Dolatyari, M. R. Yaftian and S. Rostamnia, *Sep. Sci. Technol.*, **53**, 1282 (2018).
21. L. Dolatyari, M. R. Yaftian and S. Rostamnia, *J. Environ. Manage.*, **169**, 8 (2016).
22. L. Dolatyari, M. R. Yaftian and S. Rostamnia, *J. Taiwan Inst. Chem. Eng.*, **60**, 174 (2016).
23. R. Karmakar, P. Singh and K. Sen, *Sep. Sci. Technol.*, **56**, 2369 (2021).
24. Z. Marczenko and M. Balcerzak, *Separation, preconcentration and spectrophotometry in inorganic analysis*, NetherlandS: Elsevier Science B.V, Amsterdam (2000).
25. J. Coates, *Interpretation of infrared spectra, a practical approach, encyclopedia of analytical chemistry*, R. A. Meyers (Ed.), Wiley & Sons, Chichester (2000).
26. B. Ersoy, A. Sariisik, S. Dikmen and G. Sariisik, *Powder Technol.*, **197**, 129 (2010).
27. I. Arrigo, P. Catalfamo, L. Cavallari and S. D. Pasquale, *J. Hazard. Mater.*, **147**, 513 (2007).
28. M. E. Borges, L. Hernández, J. C. Ruiz-Morales, P. F. Martín-Zarza, J. L. G. Fierro and P. Esparza, *Clean Techn. Environ. Policy*, **19**, 2113 (2017).
29. T. Umegaki, R. Ogawa, N. Toyama, S. Ohki, M. Tansho, T. Shimizu and Y. Kojima, *Inorg. Chem. Front.*, **4**, 1568 (2017).
30. M. Thommes, K. Kaneko, A. Neimark, J. Olivier, F. Rodriguez-Reinoso, J. Rouquerol and K. Sing, *Pure Appl. Chem.*, **87**, 1051 (2015).
31. Z. Ansari, S. S. Singha, A. Saha and K. Sen, *Spectrochim. Acta A Mol. Biomol. Spectrosc.*, **176**, 67 (2017).
32. P. Singh, P. K. Maiti and K. Sen, *Bull. Mater. Sci.*, **43**, 56 (2020).
33. T. Yokoyama, A. Ueda, K. Kato, K. Mogi and S. Matsuo, *J. Colloid Interface Sci.*, **252**, 1 (2002).
34. M. A. Treto-Suárez, J. O. Prieto-García, A. Mollineda-Trujillo, E. Lamazares, Y. Hidalgo-Rosa and K. Mena-Ulecia, *Sci. Rep.*, **10**, 10836 (2020).
35. C. Kannan, K. Muthuraja and M. R. Devi, *J. Hazard. Mater.*, **244-245**, 10 (2013).
36. F. Chargui, M. Hamidouche, H. Belhouchet, Y. Jorand, R. Doufnoune and G. Fantozzi, *Boletín de la Sociedad Española de Cerámica y Vidrio*, **57**, 169 (2018).
37. C. Ekberg, Y. Albinsson, M. J. Comarmond and P. L. Brown, *J. Solution Chem.*, **29**, 63 (2000).
38. J. Beardmore, X. Lopez, J. I. Mujika and C. Exley, *Sci. Rep.*, **6**, 30913 (2016).
39. K. Y. Foo and B. H. Hameed, *Chem. Eng. J.*, **156**, 2 (2010).
40. A. K. Kaygun and S. Akyil, *J. Hazard. Mater.*, **147**, 357 (2007).
41. Z. Hongxia, D. Zheng and T. Zuyi, *Colloids Surf. A Physicochem. Eng. Asp.*, **278**, 46 (2006).
42. A. Nilchi, T. S. Dehaghan and S. E. Garmarodi, *Desalination*, **321**, 67 (2013).
43. C. L. Chen and X. K. Wang, *Appl. Geochem*, **22**, 436 (2007).
44. M. O. Abd El-Magied, *J. Eng.*, **2016**, 1 (2016).
45. K. Y. Foo and B. H. Hameed,*Chem. Eng. J.*, **156**, 2 (2010).
46. A. M. Abu El-Soad, M. O. Abd El-Magied, M. S. Atrees, E. G. Kovaleva and G. Lazzara, *Int. J. Biol. Macromol.*, **139**, 153 (2019).

Supporting Information

Industrial by-product utilized synthesis of mesoporous aluminum silicate sorbent for thorium removal

Sarah Alharthi* and Mahmoud Osman Abd El-Magied,†**

*Department of Chemistry, College of Science, Taif University, P.O. Box 11099, Taif 21944, Saudi Arabia
**Department of Isotope Geology, Research Sector, Nuclear Materials Authority, P.O. Box 530, El Maadi, Cairo, Egypt
(*Received 14 April 2021 • Revised 3 June 2021 • Accepted 22 June 2021*)

Thorium Determination

Thoron I method is one of the most commonly spectrophotometric methods employed for thorium determination. Thoron I reacts with Th(IV) in an acid medium to yield a red, water-soluble complex, which forms the basis for the spectrophotometric determination.

Reagent:

1. Thoron I: 0.1% aqueous solution.
2. Ascorbic acid solution: 1% aqueous solution.
3. Stander Th(IV) solution: 1,000 ppm solution of Th(IV) was prepared by dissolving 2.46 g of $Th(NO_3)_4{\cdot}5H_2O$ in 1 L of bidistilled water acidified with 5 mL of conc. HNO_3.
4. Tartaric acid solution: 1% aqueous solution.

Procedure:

1. Place the sulfate-free sample solution in a 50-ml volumetric flask.
2. Add 2 mL of ascorbic acid solution and mix well.
3. Add 2 mL of tartaric acid solution and mix well.
4. Add 4 mL of Thoron I solution and mix well.
5. Add sufficient hydrochloric acid to make its concentration 0.25 M after dilution to the mark with bidistilled water.
6. Measure the absorbance of the colored solution at λ_{max} 540 nm, using a reagent blank solution as a reference.

Calibration Curve

To a series of 50 mL volumetric flasks add; 1, 2, 3, 4, or 5 mL of 50 ppm standard Th(IV) solution; 2 ml of ascorbic acid solution; 2 ml of tartaric acid solution; 4 ml of thoron I solution and sufficient hydrochloric acid to adjust its concentration at 0.25 M after dilution to the mark with bidistilled water. Measure the absorbance at λ_{max}=540 nm using a reagent blank as a reference (Fig. S1).

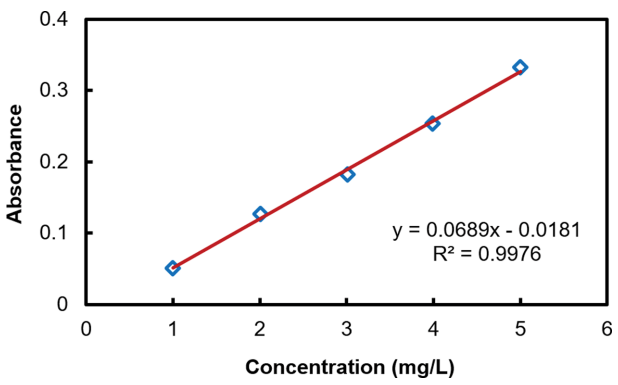

Fig. S1. Calibration curve of Th(IV) with Thoron I.

Freundlich Isotherms

Freundlich isotherm model was used to test the multilayer formation of thorium over the AS-BFS surface (Eq. (S1)).

$$\text{Freundlich isotherm: } \log q_e = \log K_F + \left(\frac{1}{n}\right)\log C_e \quad \text{(S1)}$$

Freundlich-type isotherm is classified by the term K_F (Freundlich constant adsorption) and 1/n (intensity of adsorption capacity). Values of (1/n<1) represent favorable adsorption and values (1/n)> 1 represent unfavorable adsorption. Fig. S2 shows the equilibrium isotherm obtained.

Temkin Isotherm

Temkin Isotherm is an early registered isotherm that indicates that the adsorption heat (β) is minimized linearly by increasing coverage. In the following equations, the Temkin isotherm is used.

$$q_e = \frac{RT}{b}\ln A_T + \frac{RT}{b}\ln C_e = \beta \ln A_T + \beta \ln C_e \quad \text{(S2)}$$

Using the Temkin plot of Eq. (S2) above, the constant A_T (Temkin binding constant), b (Temkin constant), and β were calculated. The value of b is 373.03, and β=6.64 (are ≤20 kJ/mol) and A_T= 2.005 confirming the physic-sorption process nature (Fig. S3).

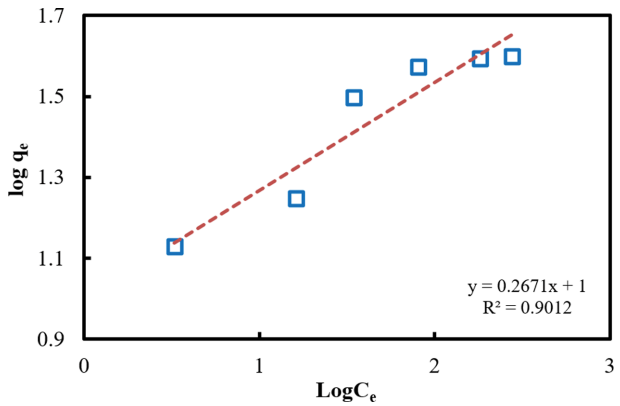

Fig. S2. Freundlich adsorption isotherm for thorium ion adsorption by AS-BFS.

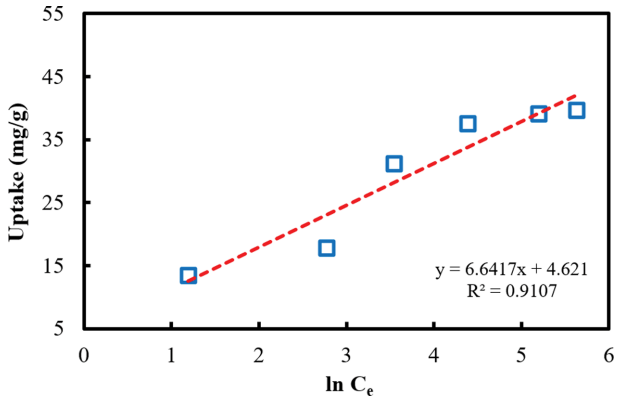

Fig. S3. Temkin adsorption isotherm for thorium ion adsorption by AS-BFS.

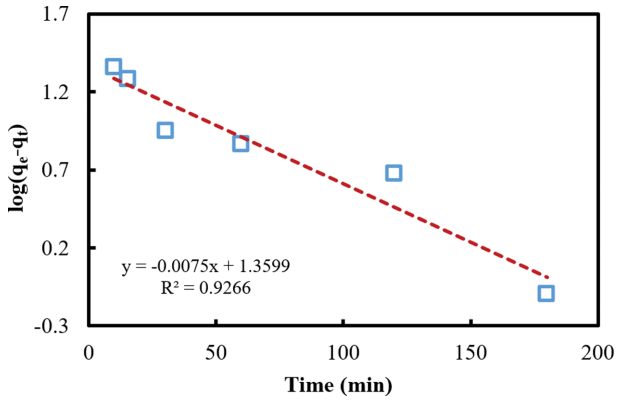

Fig. S4. Pseudo-first-order model for thorium ion adsorption by AS-BFS.

Pseudo-second Model (Lagergren Model)

The earliest model of the rate of liquid/solid adsorption was introduced in the pseudo-second model or Lagergren model, the dependence of $\log(q_e - q_t)$ with (t), Eq. (S3).

$$\log(q_e - q_t) = \log(q_1) - \frac{k_1}{2.303}t \quad \text{(S3)}$$

q_1, theoretical Lagergren capacity, and k_1 Lagergren constant were acquired from the Lagergren plot (Fig. S4, $\log(q_e - q_t)$ vs (t)).